Journal Homepage: http://ijcpe.uobaghdad.edu.iq
Iraqi Journal of Chemical and Petroleum Engineering
Vol. 25 No. 4 (December 2024) 157 – 166
EISSN: 2618-0707, PISSN: 1997-4884

Studying of high pressure/deep formations based on rock mechanical properties evaluation

Muayad Khalaf Bandar [a, *], Nagham Jasim Al- Ameri [a]

a Petroleum Engineering Department, College of Engineering, University of Baghdad, Baghdad, Iraq

Abstract

Geomechanics plays a significant role in all phases of an oil and gas field's life cycle, from exploration to production and even beyond field abandonment. It has various applications in the petroleum industry, such as predicting safe mud window and determining the magnitude and direction of in-situ stresses. The objective of this study is to determine the magnitude and orientation of far-field stresses, identify fault types, estimate pore pressure, and evaluate mechanical properties for different formations by constructing a one-dimensional geomechanical model (1D-MEM) for a deep well in the Halfaya oilfield. This study utilizes open-hole log measurements, including density, sonic compression and shear wave velocities, gamma-ray, caliper, and bit size. The results from the model indicate that the Mishrif A, Mishrif B1, Mishrif B2, Mishrif C1, Mishrif C2, Mishrif C3, Mauddud, Nahr Umr B, Ahmadi, and Zubair formations exhibit normal faulting. On the other hand, the Nahr Umr A, Shuaiba, Ratawi, and Yamama formations show strike-slip faulting. The Rumaila formation, based on the magnitudes of the far-field stresses (σv, σH, and σh), appears to exhibit reverse faulting. Furthermore, the Yamama formation demonstrates abnormally high pore pressure, while other formations are considered natural pressure formations. In terms of rock properties, shale and sand formations have lower Young's modulus, Poisson's ratio, and UCS, whereas limestone formations have higher values. Moreover, limestone formations exhibit higher friction angles compared to sandstone and shale formations.

Keywords: Halfaya Oilfield; Mechanical Earth Model; Pore Pressure; Elastic Properties; Far-field Stresses.

Received on 04/01/2024, Received in Revised Form on 21/05/2024, Accepted on 21/05/2024, Published on 30/12/2024

https://doi.org/10.31699/IJCPE.2024.4.15

1- Introduction

Geomechanics is a specialized field of engineering science that studies the relationship between stress, pressure, temperature, and various environmental factors affecting the deformation and potential failure of soil and rock formation [1]. This branch of science often explores the breaking point of these materials, leading to fracturing. According to the Geological Society of America's Committee on Rock Mechanics (GSA), rock mechanics is defined as a theoretical and practical study of how rocks behave under different mechanical conditions, and it focuses on how rocks respond to the force field present in their physical environment [2]. Rock mechanics, a subset of geomechanics, utilizes principles from continuum and solid mechanics, as well as geological sciences, to assess the reaction of rocks to external pressures. Engineering rock mechanics primarily deals with human-induced alteration to rock formations, while geological rock mechanics focuses on disturbance caused by natural geological processes. This interdisciplinary field combines elements of physics, petroleum, mathematics, geology, civil, and mining engineering [3]. The process of examining rock mechanics typically involves conducting geological and geophysical studies to determine the lithologies and boundaries of the rock types present in specific areas. This is followed by drilling or excavating to obtain core samples and estimate the mechanical properties of the rocks. Subsequent stages involve calculating far-field stresses, predicting mechanical properties, and determining geomechanical parameters [2]. The mechanical earth model (MEM) serves as a comprehensive database and algorithm that characterizes the mechanical properties of the rock, and the fractures, as well as temperature, pressure, and stresses at a certain depth [3]. This tool aids the understanding of how rock changes in shape, size, and fractures patterns due to drilling and completion, process [4]. For engineering aspects, geomechanics is considered as a fundamental that examines the distribution of stresses on rocks which can be affected by various parameters such as temperature, pressure, and environmental conditions on rocks [5]. Furthermore, Geomechanics plays a crucial role in the oil industry throughout the field's lifespan, as it essential in every stage of oil extraction, from exploration to production, and even after well abandonment. Its applications in the oil industry include estimation pore pressure, evaluating rock properties, predicting in-situ stresses, determining the safe mud window, improving wellbore stability and trajectory, and controlling sand production [6]. The main components of the MEM are

*Corresponding Author: Email: moaid.Bandr2108m@coeng.uobaghdad.edu.iq

pore pressure, mechanical properties of the rock, and far-field stresses [7]. The MEM provides important outputs like the mud weight window and well trajectory, which contribute to reducing the instability of the wellbore and thus reducing the excessive costs resulting from NPT [8]. Geomechanical problems can be reduced by constructing 1D-MEM, which in turn estimates the pore pressure, magnitude and direction of far-field stresses and also evaluates the mechanical properties of the rock [9].

2- Area of the study and its geological setting

Halfaya oilfield is one of the largest mature oilfields in southern Iraq, located in the south of Missan province, 400 kilometers south-east of Baghdad, Iraq's capital [10]. It is about 38 kilometers long and 12 kilometers wide, the majority of its terrain consists of flat, desert landscapes [11, 12]. Tertiary Jeribe and Upper Kirkuk; Upper Cretaceous Hartha; Tanuma; Khasib; Mishrif and Nahr Umr; and Lower Cretaceous Yamama are the oil-bearing formations of the Halfaya oilfield. These reservoirs are located at depths varying between 1900 and 4300 meters [13, 14]. In this study we built 1D-MEM for (HF-Y161) well to find magnitude and direction of far-field stresses, estimate pore pressure, and assess rock mechanical properties The Halfaya oil field study section extends from the Mishrif Formation (2916 m) to the Yamama Formation at a depth of about (4413 m), which include this formations (Mishrif A, Mishrif B1, Mishrif B2, Mishrif C2 ,Mishrif C3, Rumaila, Ahmadi, Mauddud, Nahr-UmrA ,Nahr-Umr B, Shauiba, Zubair, Ratawi ,Yamama), [15, 16].

3- Methodology

The geomechanical model study for the Halfaya oilfield was conducted utilizing an integrated process. The initial stage was gathering the necessary data to develop the model, such as well logs (density, gamma ray, shear wave velocities, compression wave velocities, caliper, bit size) and measured data (core mechanical laboratory tests (triaxial test), repeated formation tests (RFT), and mini-fracture testing) to check its validity. The second stage was to create a one-dimensional mechanical earth model (1D-MEM) from the log data. The third step was to compute the profiles for the 1D-MEM components such as mechanical properties of rock, pore pressure and magnitudes, and direction of far-filed stress. Finally, validation was carried out and the geomechanical model was built for well HF-Y16, focusing on segments from Mishrif Formation at a depth of 2916 m to the Yamama Formation at a depth of 4413 m.

4- Mechanical earth model

A 1D mechanical earth model is constructed using Techlog 2015 software, and raw data from the field will be analyzed to confirm the model's correctness. Vertical stress (Overburden stress), mechanical stratigraphy (shale flag), pore pressure, rock characteristics (elastic and strength), and horizontal stresses (minimum horizontal stress and maximum horizontal stress) are the primary components to build mechanical earth model (geomechincal model) for HF-Y161.

4.1. Calculation for overburden stress

Overburden stress, also known as vertical stress (Sv), is the pressure put on a point by the weight of formations that are below it and contain fluid. One of the principal strains is vertical stress, which points in the direction of the earth's core. The depth-dependent propagation of overburden pressure results in an increase in sediments [17]. The overburden stress (S_v) can be estimate from Eq. 1 in Fig. 1. The average formation bulk and pore pressure gradient may be used to compute the overburden stress [17].

$$Sv = \int_0^z \rho g\,(z)dz \quad (1)$$

Where, G is acceleration by gravity (m/s²), Z is formation depth (m), S_v is overburden pressure (psi), P is rocks' overall density.

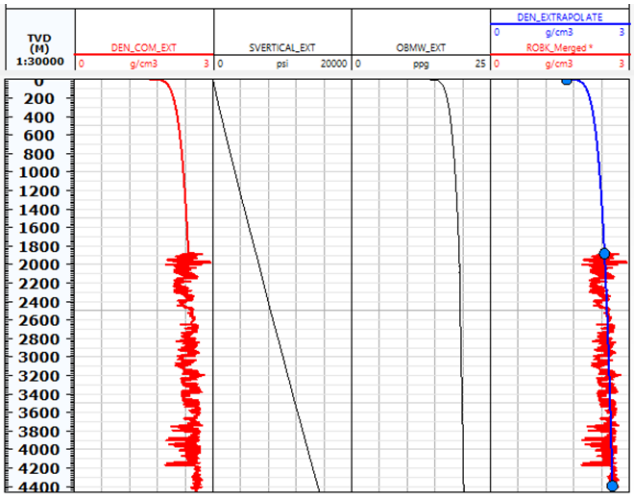

Fig. 1. Vertical stresses profile integrated from bulk density for Well HF-Y161 (Techlog Software 2015)

4.2. Mechanical stratigraphy (shale flag)

It used to differentiate between shale formation and non-shale formation [18]. The profile of shale flag was calibrated with pore pressure taken from permeable layers by using repeated formation tests (RFT) of formation test (red circle in fourth track) and show good agreement as illustrated in Fig. 2.

4.3. Pore pressure estimation

The pressure of fluids contained in porous rocks is known as pore pressure. Pore pressure (Pp) carries part of the vertical stress, whereas the other part is held by rock grains [7]. It is a crucial factor in drilling plane, petroleum production, and geomechanical modeling. It significantly affects both the wellbore's deformation and the stability

analysis of the drill hole [19]. The accuracy in prediction of pore pressure is a substantial for operation for minimizing the time to treatment the borehole problems and avoid drilling incidents such as (lost circulation, kick, blowouts). The diacritical pore pressure in shale formation may be determined using sonic and resistivity logs [19]. Pore pressure is classified into three classes according to its magnitude [19], as follows:

a. Normal pore pressure**:** This is the pressure generated by the fluid column from the formation's surface to the bottom, and it varies based on the kind of fluid, temperature gradient, gases present, and dissolved solids content, therefore it is not constant.
b. Abnormal pore pressure**:** Any pore pressure greater than the hydrostatic pressure of the forming water is considered abnormal pore pressure. Abnormal pressure is assumed to be caused by extranormal hydrostatic pressure, or increased pressure.
c. Subnormal Pore Pressure**:** The formation pressure for the stated depth is lower than the hydrostatic fluid pressure.

Pore pressure is a critical component of the 1D-MEM, and it plays a significant role in estimating the magnitude of in-situ horizontal stresses and predicting the safe mud weight window to achieve stable wellbore drilling. Estimation of pore pressure using direct and indirect approaches. Procedures, such as repeated formation testing (RFT), were used to assess the direct measuring methods. This test is applied to the well in field [20].

The most popular indirect method for determining pore pressure in the oil industry is Eaton's method. Based on various log measurements for indirectly predicting pore pressure continuously along a studied interval, Eaton presented general equation form as expressed in Eq.3, which utilized in this study to calculate the PP for the non-shale zone [21].

In this study, the profile of normal pressure (Hydrostatic pressure, Ph) was calculated using the Eq.2, and the profile of geo-pressure was calculated using the Eaton method, [20] which expresses by Eq.3. The linear interpolation method, on the other hand, was used to predict the pore pressure in permeable limestone (production section) as shown in Fig. 3 under the name (PPRS EATON S), and the resultant profile was calibrated against actual pressure point measurements from indirect methods to minimize the uncertainty of the estimated pore pressure) as shown in Fig. 3 under the name (formation pressure).

$$Ph = \int_0^z \rho_w \, g \, dz \tag{2}$$

$$\mathrm{Pp} = \sigma v - (\sigma v - \mathrm{Ph}) * a * \left(\frac{\Delta t norm}{\Delta t}\right)^n \tag{3}$$

Where, ρ_w is the water density (gm/cm^3), g is gravitational constant (9.8 m/sec^2), z is the dense water column (m), Δt is the slowness from sonic log in shale formation, "a" and "n" are fitting factors Eaton factor and Eaton exponent, respectively. The default values are a=1 and n=3, Ph is the hydrostatic pressure, $\Delta t norm$ is the normal slowness in shale formations.

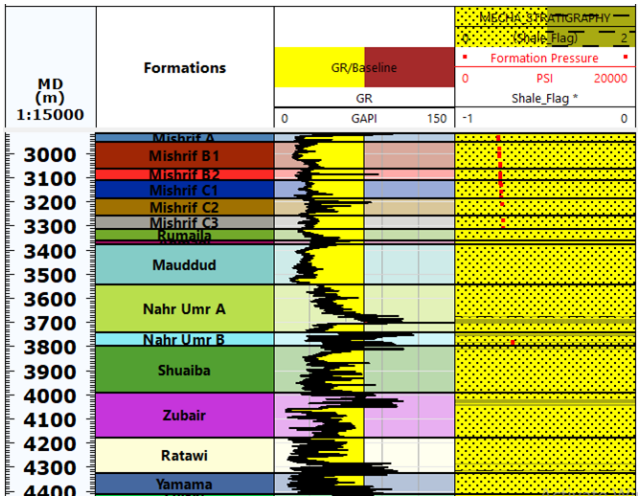

Fig. 2. Shale flag profile calibrated by pore pressure points for Well HF-Y161 (Techlog Software 2015)

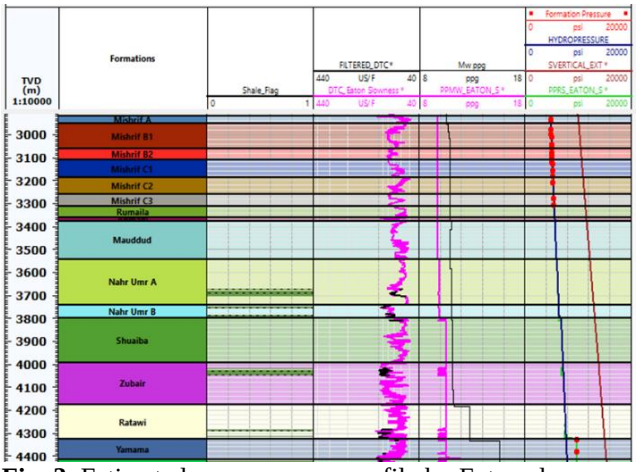

Fig. 3. Estimated pore pressure profile by Eaton slowness of HF-Y161 (Techlog Software 2015)

4.4. Rock mechanical properties

These properties are an important factor in determining the magnitude of horizontal stresses. Mechanical rock properties may be estimated using a variety of static rock tests or determined by logs such as sonic and density logs. The shear and compression slowness log of the sonic log are used to calculate the dynamic measurement. Dynamic measurements are often higher than static measurements [22]. They are divided into elastic properties and strength properties.

Elasticity is the material property that enables the rock to sustain the volume or shape deformation. Elastic properties included Young's modulus (E) (is a measure the capacity of a material to withstand changes in length during the application of longitudinal compression or strain), Poisson's ratio (v) (is measuring the rock expands with respect to a shorting in axial and the value of the ratio depends on the orientation of stresses which applied and orientation of longitudinal strain through ratio was

measured), Shear modulus (G) (is measurement the stiffness of material resistance against the applied shear stress) and Bulk modulus (K) (is measuring the capability of material to resistance the change in volume when all sides of the material are under compression), [22].

It is evaluated using direct laboratory techniques and indirect petrophysical methods, with direct methods often utilized to calibrate the estimated profiles of the property determined using indirect methods. In this study, the mechanical properties of rock were estimated using indirect petrophysical methods using three types of logs (shear and slowness velocities, bulk density) as expressed in the Eqs. 4 and 5 which were used to calculate the shear moduli (G) and bulk moduli (K), Thus, applying the Eqs. 6 and 7 consecutively, the dynamic profiles of Young's modulus (E) in Mpsi and Poisson ratio (v) unit less may be estimated from the two moduli (shear and bulk), [23].

$$G_{dyn} = 13474.45 * \frac{\rho b}{(\Delta t_{shear})^2} \quad (4)$$

$$K_{dyn} = 13474.45 * \left[\frac{\rho_b}{(\Delta t_{comp})^2}\right] - \frac{3}{4} * G_{dyn} \quad (5)$$

$$E_{dyn} = \frac{9*G_{dyn}*K_{dyn}}{G_{dyn}+3*K_{dyn}} \quad (6)$$

$$\upsilon_{dyn} = \frac{3K_{dyn}-2G_{dyn}}{6K_{dyn}+2G_{dyn}} \quad (7)$$

Where, Δt_{shear} is shear slowness of bulk formation us/ft, ρb is formation bulk density (g/cm3), $\Delta t_{comp}\ is$ compressional slowness of the bulk formation us/ft, υ_{dyn} is dynamic poisson ratio.

These dynamic properties were converted to estimation the static elastic properties by using an appropriate correlation. in this study used the correlation of John Fuller's to estimation static Young's Modulus profile (Eq. 8) [23], which describes the more realistic profile and usually lower than the dynamic profile because the influence of (pore pressure, cementation, amplitude also rate of stress-strain). The static poisson's ratio was considered as analogous to the dynamic form as usually used in rock mechanics (Eq. 9).

$$Esta = 0.032 * Edyn^{1.632} \quad (8)$$

$$\upsilon_{sta} = \upsilon_{dyn} * \text{PR multiplier} \quad (9)$$

Where, υ_{sta} is static poisson ratio, PR multiplier defaulted = 1, unit less.

Fig. 4 shows that the calculated static profiles match the direct results from laboratory tests very well.

Strength properties are the highest stress at which the sample weakens as it continues to deform. Strength properties included unconfined compressive strength **(**forces of the rock can be estimated in the laboratory from tests of the core and secondarily from the compressional velocity of sound), Friction Angle (measure of the unit rock capability to endure shear stress, when a failure occurs due to shear stress and measured among the normal force and resultant force [5], Cohesion Strength (the shear strength of rocks in the absence of normal stress [4], and Tensile Strength(when the effective tensile stress overrides the tensile strength of the sample, the tensile failure will occur and usually splits over one or tiny fracture planes [24, 25]. There are many correlations for determining USC, friction angle ($\boldsymbol{\varphi}$), cohesion strength ($\boldsymbol{So}$) and tensile strength ($\boldsymbol{T}$s), [26]. In this study the unconfined compressive strength (UCS) profile was estimated from static Young's modulus correlations profile (Eq. 10) then as a function of UCS was used to estimate the tensile strength profile (Eq. 11) and the internal friction angle profile was estimated by using a correlation of Gamma ray (Eq. 12) and cohesion strength ($\boldsymbol{So}$) estimated by (Eq. 13).

$$UCS = 331 + 0.0041\ Esta \quad (10)$$

$$\text{TS=UCS*k} \quad (11)$$

$$\varphi = 57.8 - 105\ GR \quad (12)$$

$$S_o = \frac{UCS}{2tan\emptyset} \quad (13)$$

Where, GR is gamma ray log readings, USC is unconfined compressive strength, $\emptyset$ is friction angle, TS is tensile strength , S_o is cohesion strength , $Estat$ is static young's modulus, K is facies and zone-based factor which adjusted till get the better matching with core laboratory test , K default value is 0.1unit less.

As shown in Fig. 5, the calculated profile of the rock mechanical strength parameters shows a good matching with the direct results of the core laboratory tests.

Dynamic measurements of rock properties are often greater than static measurements due to several factors. Here are reasons why dynamic measurements may yield higher values:

a. Stress Redistribution: Dynamic measurements involve subjecting the rock sample to dynamic loading conditions, such as impact or vibration. These loading conditions induce stress redistribution within the rock mass, leading to increased effective stress and higher measured values of rock properties. In contrast, static measurements apply constant stress without significant redistribution, which may underestimate the true strength or stiffness of the rock.
b. Time-Dependent Behavior: Rocks can exhibit time-dependent behavior, known as viscoelasticity or creep. Dynamic measurements account for the influence of time by subjecting the rock sample to varying loading rates. This allows for the assessment of instantaneous and time-dependent responses, capturing the higher values associated with dynamic loading. Static measurements, on the other hand, do not consider the effects of time and may not fully capture the viscoelastic behavior of the rock.
c. Strain Rate Sensitivity: Many rocks exhibit strain rate sensitivity, meaning their mechanical properties can vary depending on the rate at which they are deformed. Dynamic measurements involve higher

strain rates compared to static measurements, which can activate rate-dependent mechanisms within the rock structure.

Fig. 4. Dynamic profile and static profile of rock elastic properties for HF-Y161 (Techlog Software 2015)

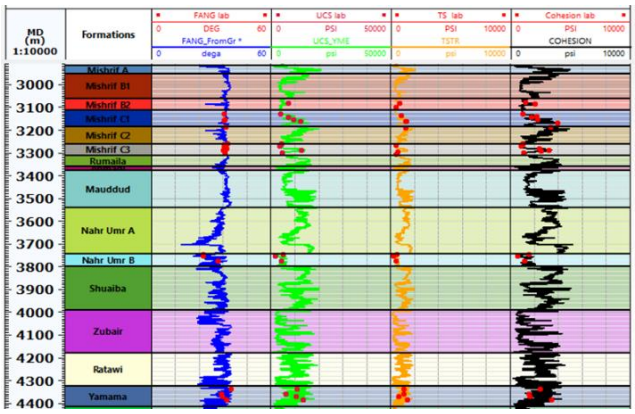

Fig. 5. Profiles of strength properties for HF-Y161 (Techlog Software 2015)

4.5. Magnitude and direction for horizontal stresses

The horizontal stresses are influenced by the overburden stress action on the rock. The maximum and minimum horizontal stresses in an anisotropic deposit devoid of tectonic activity have the same magnitude ($\boldsymbol{\sigma h}$ = $\boldsymbol{\sigma}$H). Otherwise, horizontal stresses will be greater due to an active area with faulting or mountains [4].

Minimum Horizontal Stress ($\boldsymbol{\sigma h}$) is important in engineering and an important parameter in the petroleum industry because it is used to evaluate (ideally mud weight, casing set points, selecting appropriate trajectories, etc.) and solve borehole instability problems [27]. Maximum Horizontal Stress ($\boldsymbol{\sigma}$H) is a critical metric in the petroleum industry and geologic sciences. There is no direct method to estimate the magnitude of maximum horizontal stress, therefore, numerous methods have been developed to calculate the magnitude of maximum horizontal stress [28].

In many geomechanics events the magnitude and direction of horizontal stresses are crucial. Direct methods for estimating the minimum horizontal stress include the leak-off test, the hydraulic fracturing test, and the min-frac test [29]. In this study Mohr-coulomb stress model (Fig. 6) and the Poroelastic horizontal stress model (Fig. 7) were utilized to compute the maximum and minimum horizontal stress. Mohr-Coulomb stress model was utilized to compute the maximum and minimum horizontal stress as a function of the friction angle, vertical stress, and pore pressure by Eqs. 14 and 15.

$$\sigma_h = (\sigma v - \alpha\, pp)/tan^2\left(\frac{\pi}{4}+\frac{\theta}{2}\right)+ \alpha\, pp \quad (14)$$

$$\sigma_H = tan^2\left(\frac{\pi}{4}+\frac{\theta}{2}\right) * (\sigma v - \alpha\, pp) + \alpha\, pp \quad (15)$$

The method for calculating horizontal stresses that was most frequently employed was the poroelastic horizontal stress model. The poroelastic horizontal stress technique makes use of the overburden stress, pore pressure, static Young's modulus, Poisson ratio, and Biot's constant by Eqs. 16 and 17, as shown in the equation below.

$$\sigma h = \frac{\nu}{1-\nu} * \sigma v - \frac{\nu}{1-\nu} * \alpha Po + \alpha Po \frac{S*\nu}{1-\nu} * \varepsilon h + \frac{E*\nu}{1-\nu^2} * \varepsilon H \quad (16)$$

$$\sigma H = \frac{\nu}{1-\nu} * \sigma v - \frac{\nu}{1-\nu} * \alpha Po + \alpha Po \frac{S*\nu}{1-\nu} * \varepsilon H + \frac{E*\nu}{1-\nu^2} * \varepsilon h \quad (17)$$

Where, α is biot's coefficient, E is young's modulus in static form, Po is pore pressure, υ is poisson's ratio in static form, ε_h and ε_H are tectonic strains, they determine by Eqs. 18 and 19.

$$\varepsilon h = \frac{\sigma v * \nu}{E} * \left(1 - \frac{\upsilon^2}{1-\upsilon}\right) \quad (18)$$

$$\varepsilon H = \frac{\sigma v * \nu}{E} * \left(\frac{\upsilon^2}{1-\upsilon} - 1\right) \quad (19)$$

One of the geophysical logs, a four-arm caliper, the Formation Micro Image (FMI), and the micro seismic focal mechanism (innovative technology) may be used to ascertain the direction of stress. The instruments that are still most often used are the caliper and the FMI [30]. The Formation Micro Imager (FMI) indicates that the maximum horizontal stress orientation in the Halfaya oilfield is around N20-35 E [31].

4.6. Far-field stress magnitudes related to the fault regimes

In-situ stresses described the condition of the rock prior to human activity such as drilling [4]. Four parameters ((σv, σH and σh) and stress orientation) must be described to understand the state of stress in depth [24]. According to the relationship between stress and faulting theory, there are three in-situ stress faulting regimes. Anderson (1951) theory assumes faults are created by shear failure which in-situ stress causes. Anderson presented a categorization of the fault regime with a difference in-situ principal stress. In-situ stresses are maximum, intermediate, and minimum. Fault regimes may be classified into three types based on the connection between primary stresses and shear failures [7]. Normal

faulting regime when $\sigma v > \sigma H > \sigma h$ and strike-slip faulting regime when $\sigma H > \sigma v > \sigma h$ and reverse faulting regime when $\sigma H > \sigma h > \sigma v$ [7].

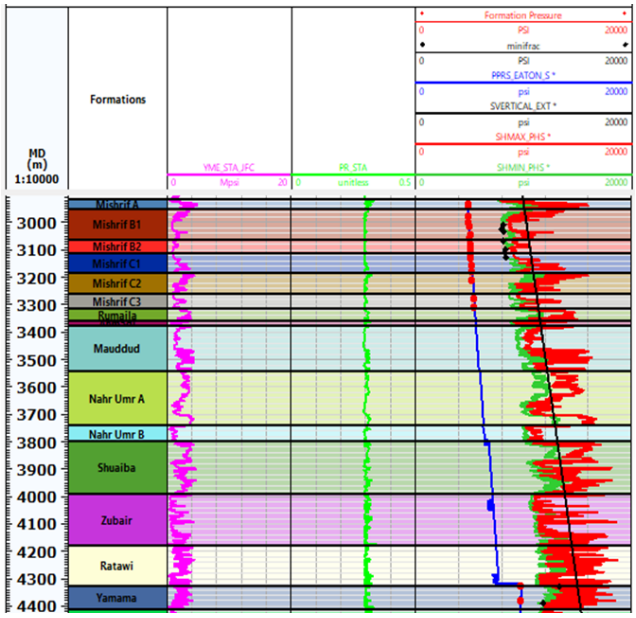

Fig. 6. Maximum and minimum horizontal stresses measured by Poro-Elastic horizontal strain model for HF-Y161(Techlog Software 2015)

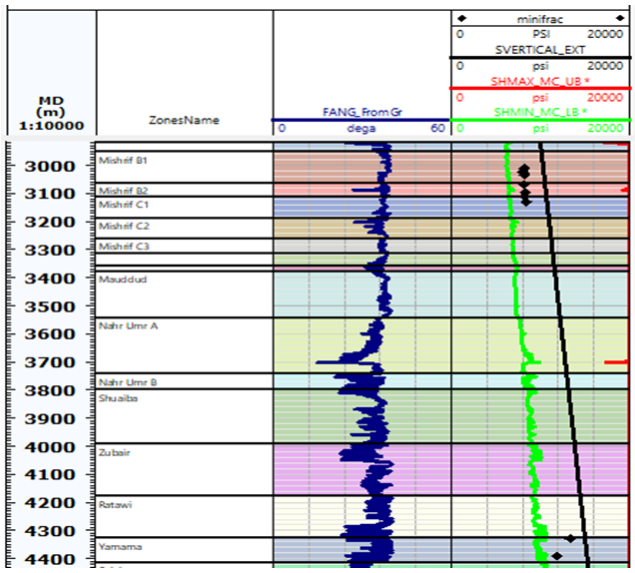

Fig. 7. Maximum and minimum horizontal stresses measured by Mohr-Coulomb model for HF-Y161 (Techlog Software 2015)

4- Results and discussion

Pore pressure and far-field stresses (σv, σH, and σh) and rock properties as a function of depth were computed using the mechanical earth model. As seen in Fig. 8, field data for vertical well HF-Y161 are chosen from the Halfaya oilfield to construct 1D-MEM. The results appeared as follows based on Fig. 8 and Table 1:

a. Yamama formation of Halfaya oilfield is abnormal pore pressure formation, On the contrary, other formations are natural pressure formations.

b. (Mishrif C1, Mishrif C2, Mishrif A, Mishrif B1, Mishrif B2, Mishrif C3, Mauddud, Nahr Umr B, Ahmadi and Zubair) are normal fault formations and (Nahr Umr A, Shuaiba, Ratawi and Yamama) are Strike-slip fault formations and Rumaila formation is Reverse fault depending on far-field stress (σv, σH and σh).

c. The results showed a clear heterogeneity in rock properties:

1. Young's modulus has a moderate value in shale (Mishrif C1,Mishrif C2, Mishrif C3, Nahr Umr B) formations are (1.01-1.05) MPsi, low value in claystone (Zubair , Ratawi) formations are (0.62-0.75) Mpsi ,and high value in limestone (Nahr Umr A, Mishrif B1, Mishrif B2 ,Mauddud, Shuaiba ,Ahmadi, Rumaila, Yamama) formations are (1.46-3.46) MPsi, while product formation (Mishrif A) has low value although it is consist of limestone about 0.2 MPs, because it contains hydrocarbons which caused decrease the value of Young modulus.

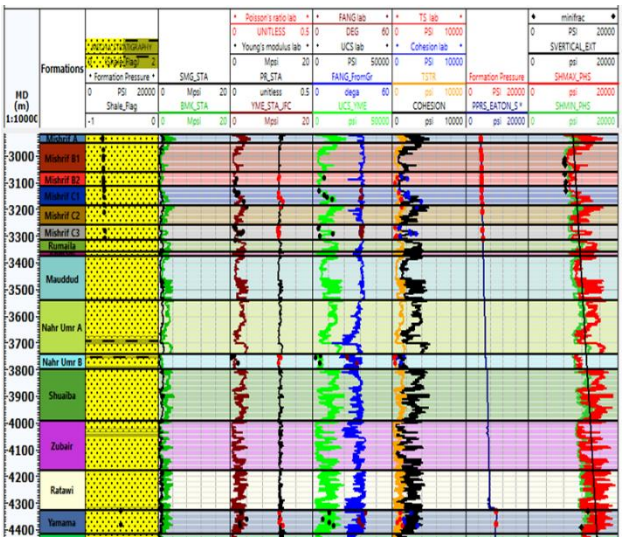

Fig. 8. 1D- mechanical Earth model (MEM) profile for HF-Y161 (Techlog Software 2015)

2. Poisson's ratio has a moderate value in shale (Mishrif C1, Mishrif C2 ,Mishrif C3, Nahr Umr B) formations are (0.292-0.295), low value in claystone (Zubair , Ratawi) formations are (0.225-0.229) ,and high value in limestone (Nahr Umr A, Mishrif B1, Mishrif B2, Mauddud, Shuaiba , Ahmadi, Rumaila ,Yamama) formations are (0.295-0.304) ,while product formation (Mishrif A) has moderate value although it is consisting of limestone about 0.291, because it contains hydrocarbons which caused decrease the value of Poisson's ratio.

3. UCS has high values in limestone (Nahr Umr A, Mishrif B1, Mishrif B2, Mauddud, Shuaiba, Ahmadi, Rumaila, Yamama) formations are (3745-14707) MPsi, while low value in claystone (Zubair , Ratawi) formations are (2490-3629) MPsi and moderate values in shale (Mishrif C1, Mishrif C2, Mishrif C3, Nahr Umr B) formations are (4174-4498) MPsi, also has low value in

produce formation **(** Mishrif A**)** although it is consisting of limestone about 1500 MPsi because it contains hydrocarbons which causes decrease in value of USC.

4. Friction angle has high values in limestone (Nahr Umr A, Mishrif B1, Mishrif B2**,** Mauddud**,** Shuaiba**,** Ahmadi**,** Rumaila**,** Yamama) formations are (37.1-38.4°) MPsi, while low values in claystone (Zubair , Ratawi) formations are (24.1°-33.2°) and moderate values in shale Mishrif C1**,** Mishrif C2**,** Mishrif C3**,** Nahr Umr B) formations are (33.6°-37.1°) MPsi ,also has a moderate value in produce formation **(**Mishrif A) about 36.7° although it is consisting of limestone because it contains hydrocarbons which causes decrease the value of friction angle.

Table 1. Results of the geomechanical properties of each formation for HF-Y161 Well

NO.	Formation	Pp	PR_STA	YME	TS	UCS	FA	S_o
1	Mishrif A	5000	0.291	0.2	100	1500	36.7	328
2	Mishrif B1	5000	0.295	2.98	385	3745	38.4	923
3	Mishrif B2	5000	0.295	1.46	467	4179	37.8	1005
4	Mishrif C1	5367.2	0.293	1.05	605	4174	37.1	1873
5	Mishrif C2	5400	0.292	1.02	1280	4271	36.6	3169
6	Mishrif C3	5400	0.292	1.01	501	4498	36.8	1102
7	Rumaila	5400	0.304	3.46	1428	13740	37.4	3508
8	Ahmadi	5568	0.296	2.69	358	6933	37.1	746
9	Mauddud	5800	0.295	1.45	618	6863	37.8	1496
10	Nahr Umr A	6197.9	0.298	3.45	1494	14707	34.8	3841
11	Nahr Umr B	6217.4	0.295	1.03	462	4458	33.7	1281
12	Shuaiba	7000	0.301	3.31	1400	14147	33.5	3385
13	Zubair	7377.2	0.225	0.62	298	2490	33.2	706
14	Ratawi	7574	0.229	0.75	922	3629	24.1	2851
15	Yamama	12533	0.298	2.66	1128	11400	38.4	1873

5- Conclusion

This study was conducted to evaluate the mechanical properties of rocks from the Mishrif formation to the Yamama formation, as well as to investigate and determine the magnitude and direction of far-field stresses on recognized fault types. The study also aimed to estimate abnormal pore pressure. The following conclusions were reached:

a. To achieve an accurate 1D-MEM, it was necessary to gather information from integrated well logs (caliper log, bit size, sonic log, gamma ray and bulk density), drilling formation data (daily drilling report, final drilling report, geological report), and field pore pressure measurement.
b. A strong correlation was found between the rock mechanical parameters calculated by correlations and the measured data (core mechanical laboratory tests such as triaxial test, repeated formation tests (RFT), and mini-fracture testing).
c. The study demonstrated that poroelastic horizontal strain model method is more accurate than mohr-coulomb stress model method when calculating the horizontal stresses.
d. The Eaton method is used to measure the natural pressures of the formations, resulting in an inconsistency between pressure measurements using the RFT test and the Eaton method in the Yamama Formation. The RFT test measures pressures of the formations regardless of the type of pressure, while the Eaton method only measures the natural pressures of formations.

Nomenclature

1D-MEM Model	One-Dimensional Mechanical Earth
FMI	Formation Micro Imager.
RFT	Repeated Formation Test
σv	Vertical stress.
σH	Maximum Horizontal Stress.
σh	Minimum Horizontal Stress.
Pp	Pore Pressure.
FANG, $\boldsymbol{\varphi}$	Friction Angle.
USC	Unconfined Compressive Strength.
TS	Tensile Strength.
S_o	Cohesion Strength.
YME	Young's Modulus.
PR_STA	Static Poisson Ratio.

References

[1] D.F. Boutt, B.K Cook, and J.R Williams, "A coupled fluid–solid model for problems in geomechanics: Application to sand production," *International Journal for Numerical and Analytical Methods in Geomechanics*, vol.35, pp. 997-1018, 2011. https://doi.org/10.1002/nag.938

[2] A.M. Al-Ajmi and R.W. Zimmerman, "Stability analysis of vertical boreholes using the Mogi–Coulomb failure criterion," *International Journal of Rock Mechanics and Mining Sciences*, vol 43, pp .1200-1211, 2006. https://doi.org/10.1016/j.ijrmms.2006.04.001

[3] S. Gstalder and J. Raynal, "Measurement of Some Mechanical Properties of Rocks and Their Relationship to Rock Drillability," *Journal of Petroleum Exploration and Production Technology*, vol. 18, no. 08, pp. 991–996, 1966. https://doi.org/10.2118/1463-PA

[4] A.Z. Noah, M.A. Mesbah, and H. Osman, "Comprehensive Wellbore Instability Management by Determination of Safe Mud Weight Windows Using Mechanical Earth Model, Meleiha Field, Western Desert, Egypt," *Egyptian Journal of Chemistry*, vol. 66, pp. 449-463, 2023. https://doi.org/10.21608/ejchem.2022.150856.6534

[5] W. B. Bradley, "Failure of inclined boreholes," *Journal of Energy Resources Technology*, vol. 101, no. 4, pp. 232–239, 1979. https://doi.org/10.1115/1.3446925

[6] R.R. Hillis and A.F. Williams, "The stress field of the North West Shelf and wellbore stability," *Journal of the Australian Petroleum Production & Exploration Association*, vol. 33, pp.373–385., 1993. https://doi.org/10.1071/AJ92028

[7] C. Chandong, M. D. Zoback, and A. Khaksar, "Empirical Relations between Rock Strength and Physical Properties in Sedimentary Rocks," *Journal of Petroleum Science and Engineering*, vol.51, pp.223–237, 2006. https://doi.org/10.1016/j.petrol.2006.01.003

[8] M. Abdulaziz., L. Hayder, A. Abdel Sattar, S. Alhussainy, and A.K. Abbas, "3D Mechanical Earth Model for Optimized Wellbore Stability, a Case Study from South of Iraq," *Journal of Petroleum Exploration and Production Technology*, vol.11, pp. 3409–3420, 2021. https://doi.org/10.1007/s13202-021-01255-6

[9] W. Al-Kattan and N. Jasim Al-Ameri, "Estimation of the Rock Mechanical Properties Using Conventional Log Data in North Rumaila Field," *Iraqi Journal of Chemical and Petroleum Engineering*, vol. 13, no. 4, pp. 27–33, 2012. https://doi.org/10.31699/IJCPE.2012.4.3

[10] W. I. T. Al-Rubaye and S. M. Hamd-Allah, "A High Resolution 3D Geomodel for Giant Carbonate Reservoir- A Field Case Study from an Iraqi Oil Field", *Journal of Engineering*, vol. 26, no. 1, pp. 160–173, 2019. https://doi.org/10.31026/j.eng.2020.01.12

[11] W. A. N. G Jun., G. U. O. Rui., Z. H. A. O. Limin., L. I. Wenke., Z. H. O. U. Wen., D. U. A. N. Tianxiang, "Geological features of grain bank reservoirs and the main controlling factors: A case study on Cretaceous Mishrif Formation, Halfaya Oilfield, Iraq", *Journal of Petroleum Exploration and Development*, vol. 43, no.3, pp. 404-415, 2016. https://doi.org/10.1016/S1876-3804(16)30047-7

[12] Y. Zhong., X. Tan., L. Zhao., D. Xiao, "Identification of facies-controlled eogenetic karstification in the Upper Cretaceous of the Halfaya oilfield and its impact on reservoir capacity", *Geological Journal*, vol. 54, no.1, pp. 450-465, 2019. https://doi.org/10.1002/gj.3193

[13] H. B. Ghalib., A. B. Al-Hawash., W. R. Muttashar., A. Bozdag., A. A. Al-Saady, "Determining the effect of mineral scaling formation under different injection water sources on the performance of Mishrif carbonate reservoir in Halfaya oilfield, Southern Iraq", *Journal of Petroleum Exploration and Production Technology*, vol. 13, no.5, pp. 1265-1282, 2023. https://doi.org/10.1007/s13202-023-01614-5

[14] M. E. Nasser, "3D Facies Modeling of Mishrif Reservoir in Halfaya Oil Field", *Iraqi Journal of Science*, pp. 180-191, 2021, https://doi.org/10.24996/ijs.2021.62.1.17

[15] S. A. Jassam and O. Al-Fatlawi, "Development of 3D geological model and analysis of the uncertainty in a tight oil reservoir in the Halfaya Oil Field", *The Iraqi Geological Journal*, pp. 128-142, 2023. https://doi.org/10.46717/igj.56.1B.10ms-2023-2-18

[16] S. W. Al-Marsomy and T. K. Al-Ameri, "Petroleum system modeling of Halfaya oil field south of Iraq" *Iraqi Journal of Science*, pp. 1446-1456, 2015.

[17] J. S. Bell, "Practical Methods for Estimating in Situ Stresses for Borehole Stability Applications in Sedimentary Basins," *Journal of Petroleum Science and Engineering*, vol.38, pp.111–119, 2003. https://doi.org/10.1016/S0920-4105(03)00025-1

[18] R.T. Ewy, "Wellbore-Stability Predictions by Use of a Modified Lade Criterion," *SPE Drill & Compl*, vol. 14, pp. 85–91, 1999, https://doi.org/10.2118/56862-PA

[19] V. Rasouli, Z. J. Pallikathekathil, and E. Mawuli, "The Influence of Perturbed Stresses near Faults on Drilling Strategy: A Case Study in Blacktip Field North Australia," *Journal of Petroleum Science and Engineering*, vol.76, pp.37–50, 2011. https://doi.org/10.1016/j.petrol.2010.12.003

[20] R. A. Plumb and S. H. Richard, "Stress-induced borehole elongation: A comparison between the four-arm dipmeter and the borehole televiewer in the Auburn Geothermal Well," *Journal of Geophysical Research*, vol. 90, pp. 5513–5521, 1985. https://doi.org/10.1029/JB090iB07p05513

[21] R.H Allawi and M.S. Al-Jawad, "Wellbore instability management using geomechanical modeling and wellbore stability analysis for Zubair shale formation in Southern Iraq," *Journal of Petroleum Exploration and Production Technology*, vol.11, pp. 4047–4062, 2021. https://doi.org/10.1007/s13202-021-01279-y

[22] A.R. Najibi, M. Ghafoori, and G. R. Lashkaripour, "Reservoir Geomechanical Modeling: In-Situ Stress, Pore Pressure, and Mud Design," *Journal of Petroleum Science and Engineering*, vol.151, pp.31–39, 2017. https://doi.org/10.1016/j.petrol.2017.01.045

[23] F. H. AlShibli and A. A. A. A. Alrazzaq, "Laboratory Testing and Evaluating of Shale Interaction with Mud for Tanuma Shale formation in Southern Iraq," *Iraqi Journal of Chemical and Petroleum Engineering*, vol. 23, no. 3, pp. 35–41, 2022. https://doi.org/10.31699/IJCPE.2022.3.5

[24] M. Hoseinpour and M.A. Riahi, "Determination of the mud weight window, optimum drilling trajectory, and wellbore stability using geomechanical parameters in one of the Iranian hydrocarbon reservoirs," *Journal of Petroleum Exploration and Production Technology*, vol.12, pp. 63–82, 2022. https://doi.org/10.1007/s13202-021-01399-5

[25] N. J. Al-Ameri, "Kick tolerance control during well drilling in southern Iraqi deep wells", *Iraqi Journal of Chemical and Petroleum Engineering*, vol. 16, no. 3, pp. 45–52, 2015, https://doi.org/10.31699/IJCPE.2015.3.5

[26] A. K. AlHusseini and S. M. Hamed-Allah, "Estimation Pore and Fracture Pressure Based on Log Data; Case Study: Mishrif Formation/Buzurgan Oilfield at Iraq," *Iraqi Journal of Chemical and Petroleum Engineering*, vol. 24, no. 1, pp. 65–78, 2023. https://doi.org/10.31699/IJCPE.2023.1.8

[27] J. S. Bell, "Practical methods for estimating in situ stresses for borehole stability applications in sedimentary basins," *Journal of Petroleum Science and Engineering*, vol. 38, pp. 111–119, 2003. https://doi.org/10.1016/S0920-4105(03)00025-1

[28] L.S. Miroshnikova, "Use of the rock preservation scale in geomechanical investigations and construction," *Journal of Hydrotechnical Construction*, vol.21, pp.72–78, 1987. https://doi.org/10.1007/BF01424908

[29] W. Khyrie and A. A. A. A. Alrazzaq, "Determination of Safe Mud Weight Window in Rumaila Oilfield, Southern Iraq," *The Iraqi Geological Journal*., vol. 54, pp. 48–61, 2021. https://doi.org/10.46717/igj.54.2F.5ms-2021-12-22

[30] D. Moos, P. Peska, T. Finkbeiner, and M. Zoback, "Comprehensive wellbore stability analysis utilizing Quantitative Risk Assessment," *Journal of Petroleum Science and Engineering*, vol. 38, pp. 97–109, 2003, https://doi.org/10.1016/S0920-4105(03)00024-X

[31] M. I. Saddam and G. M. Farman, "Estimation of Pore Pressure and In-Situ Stresses for Halfaya Oil Field: A Case Study," *Texas Journal of Engineering and Technology*, vol. 13, pp. 1–7, 2022.

دراسة التكوينات العميقة ذو الضغط العالي بالاعتماد على تقييم الخواص الميكانيكية للصخور

مؤيد خلف بندر [١، *]، نغم جاسم العامري [١]

١ قسم هندسة النفط، كلية الهندسة، جامعة بغداد، بغداد، العراق

الخلاصة

تهتم الجيوميكانيك بأي نوع من تشوه الأرض حيث تلعب دورا هاما في جميع مراحل دورة حياة حقل النفط والغاز، بدءا من الاستكشاف إلى الإنتاج وحتى ما بعد التخلي عن الحقل. بالإضافة إلى ذلك، فإن له تطبيقات متنوعة في صناعة البترول مثل التنبؤ بنافذة الطين الآمنة وحجم واتجاه الضغوط في الموقع. الهدف من هذا البحث هو تحديد حجم واتجاه ضغوط المجال البعيد، وتحديد أنواع الصدوع المختلفة، وتقدير الضغط المسامي، وتقييم الخواص الميكانيكية للتكوينات المختلفة من خلال بناء نموذج جيوميكانيكي أحادي البعد (D-MEM١) لبئر عميق . تم إجراء الدراسة باستخدام قياسات مجسات الابار مثل الكثافة والتسجيل الصوتي وسرعات موجة القص وأشعة جاما والكاليبر وقطر البريمة.

توضح نتائج النموذج الجيوميكانيكي أن تكوينات مشرف أ، مشرف ب١، مشرف ب٢، مشرف ج١، مشرف ج٢، مشرف ج٣، مودود، نهرعمرب, الأحمدي والزبير هي طبقات ذو فالق عادي بينما نهر عمر أ والشعيبة ورطاوي واليمامة هي طبقات ذو فالق انزلاقي من ناحية أخرى يبدو أن طبقة الرميلة هي طبقة ذو فالق معكوس وذلك اعتمادا على مقادير إجهادات المجال البعيد (σv، σH، σh). ووفقاً لتقدير الضغط الناتج فان طبقة اليمامة ذو ضغطاً مساميا غير طبيعي و أظهرت الخواص الصخرية المحسوبة لمعامل يونغ الساكن ونسبة بواسون وUCS قيما أقل في الطبقات الصخرية والرملية، بينما سجلت قيم أعلى في الطبقات الجيرية, بينما زاوية الاحتكاك كانت قيم عالية في الطبقات الجيرية وقيم متوسطة في الطبقات الرملية، بينما قيم منخفضة يتم تسجيلها في الطبقات الصخرية.

الكلمات الدالة: حقل الحلفاية النفطي، النموذج الأرضي الميكانيكي، الضغط المسامي، الخواص المرنة، إجهادات المجال البعيد.